ACS APPLIED MATERIALS & INTERFACES

Research Article

www.acsami.org

Versatile, Reversible, and Reusable Gel of a Monocholesteryl Conjugated Calix[4]arene as Functional Material to Store and Release Dyes and Drugs Including Doxorubicin, Curcumin, and Tocopherol

Anil Kumar Bandela, Vijaya Kumar Hinge, Deepthi S. Yarramala, and Chebrolu Pulla Rao*

Bioinorganic Laboratory, Department of Chemistry, Indian Institute of Technology Bombay, Powai, Mumbai 400076, India

Supporting Information

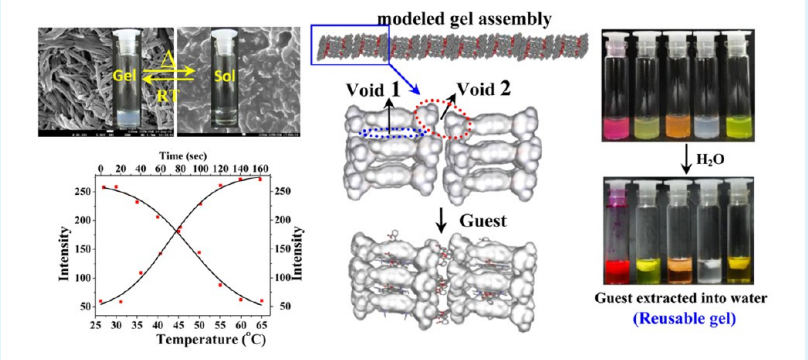

ABSTRACT: Gels are interesting soft materials owing to their functional properties leading to potential applications. This paper deals with the synthesis of monocholesteryl derivatized calix[4]arene (**G**) and its instantaneous gelation at a minimum gelator concentration of 0.6% in 1:1 v/v THF/acetonitrile. The gel shows remarkable thermoreversibility by exhibiting $T_{gel \rightarrow sol}$ at ∼48 °C and is demonstrated for several cycles. The gel shows an organized network of nanobundles, while that of the sol shows spherical nanoaggregates in microscopy. A bundle with ∼12 nm diameter possessing hydrophobic pockets in itself is obtained from computationally modeled gel, and hence the gel is suitable for storage and release applications. The guest-entrapped gels exhibit the same microstructures as that observed with simple gels, while fluorescence spectra and molecular mechanics suggests that the drug molecules occupy the hydrophobic pockets. All the entrapped drug molecules are released into water, suggesting a complete recovery of the trapped species. The reusability of the gel for the storage and release of the drug into water is demonstrated for four consecutive cycles, and hence the gel formed from **G** acts as a functional material that finds application in drug delivery.

KEYWORDS: *monocholesteryl derivatized calix[4]arene, material storage and release, drug encapsulation and release, AFM and SEM, molecular modeling*

INTRODUCTION

Although the polymer-based gels have been known for a long time, the recent focus is on low molecular-weight gelators (LMWGs) as functional materials due to their prominent properties and potential real life applications.[1−8] Unlike chemical gels, in which the gelator molecules are cross-linked via covalent bonds, the physical gels formed from LMWGs generally self-organize through noncovalent interactions.[9−17] Thus, in the case of physical gels, it is possible to bring the reversibility in self-organized structures by a suitable external stimulus, e.g., temperature, pH, mechanical stress, light irradiation, etc.[18−22] Therefore, such gels are important because of their applications in drug delivery, gas storage, sensing, and several other materials-based applications, e.g., self-healing materials.[23−26] The quest for new molecular systems continues to be a thrust activity particularly those possessing the requisite features to form functional gels. In the literature, various molecular scaffolds have been explored as gelators, and some common ones among these are cholesteryl derivatives, peptides, functionalized porphyrins, and pthalocyanins.[27−34] Thus, the choice of calixarene conjugates as gelators opens new vistas in material chemistry since these can provide a variety of noncovalent interactions including hydrogen bonding, $\pi\cdots\pi$, hydrophobic, and van der Waals type via suitable functionalization either at its upper rim or at its lower rim. Additionally, these conjugates provide hydrophobic cavity that would be important in holding a guest or a drug molecule.[34] However, the use of calixarenes as gelators has been scarce in the literature, and only few reports have appeared recently.[35−40] For example, a bisamide-linked dicholesteryl-based calix[4]-arene forms a gel in a mixture of 1:1 *n*-decane−acetonitrile and exhibits fully reversible thixotropic properties, a phenomenon

Received: March 21, 2015
Accepted: May 6, 2015
Published: May 6, 2015

DOI: 10.1021/acsami.5b02506
ACS Appl. Mater. Interfaces 2015, 7, 11555−11566

Scheme 1. Synthesis of G[a]

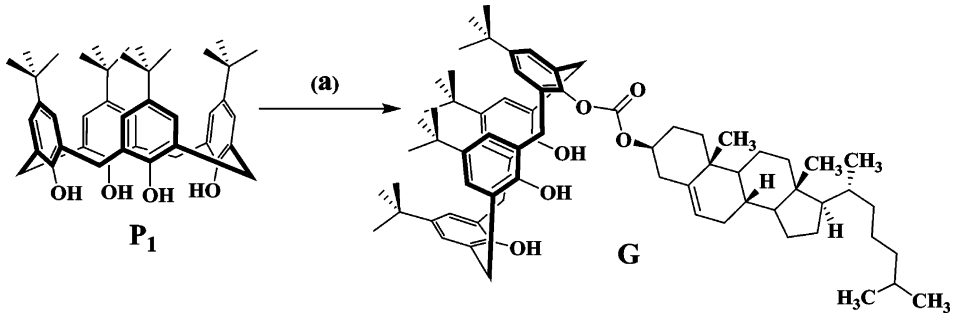

[a](a) Cholesteryl chloroformate, K_2CO_3, NaI, dry acetone, reflux for 15 h.

that was never reported before.[41] However, a similar pair of molecules of dicholesteryl-based calix[4]arene connected through L- or D-phenylalanine shows the effect of chirality on the gelation behavior. Among the L- or D-gelator systems, the latter forms a stable gel in isopropanol where sonication enhances the strength of the gel.[42] The suitability of the calix[4]arene platform in forming the gel has been shown in the case of 9,10-bisisoxazolylanthracene and thienyl-2,5-bisisoxazolylmethylbiscalix[4]arene.[43,44] Of these, the first one is thermoresponsive and emits blue light, and the second one displays phase-selective gelation for the recovery of oil spills. When calix[4]arene is di- or tetra-derivatized with cholesterol, the conjugates exhibit liquid crystalline behavior rather than forming a gel.[45] In order to find real life applications, the gelators need to gelate a broad variety of solvent media with low critical gelator concentration (CGC), while the reversibility brought by the external stimuli would add to its advantage. Therefore, herein we report the synthesis of a cholesteryl monoderivative of calix[4]arene that forms gel instantaneously at low CGC and demonstrate its functional characteristics, such as storage and release of dyes and drug molecules, reversibly.

RESULTS AND DISCUSSION

Synthesis of the Carbonate-Linked Monocholesteryl Conjugate of Calix[4]arene. The organogelator **G** has been synthesized by one-step condensation of chloroformyl cholesterol with *p-tert*-butyl calix[4]arene as per that shown in Scheme 1. The product **G** has been characterized satisfactorily by ^{1}H and ^{13}C NMR, ESI MS, FTIR, and elemental analysis.

Visual Gelation. The calix conjugate, **G**, has been found to form a gel instantaneously in different solvent systems at room temperature. In order to proceed for the gelation studies, the solubility of the **G** has been checked in 20 common organic solvents. The **G** is soluble in nonpolar aprotic solvents; however, it is insoluble in both protic and nonprotic polar solvents. The **G** dissolved in solvents like dichloromethane, chloroform, tetrahydrofuran, toluene, or diethyl ether exhibits gelation upon addition of acetonitrile. In some cases, the gelation was induced by the addition of dimethyl sulfoxide, dimethylformamide, methanol, or ethanol. However, the gelation was not observed with the solvents with bulky substituents, such as isopropanol, *t*-butanol, and ethyl acetate. The results of the gelation are summarized in Table S1, and the corresponding photographic images were provided in Figure S2 of the Supporting Information.

It is important to note that only the **G** showed gelation, whereas the corresponding precursors, viz., cholesteryl chloroformate or the simple *p-tert*-calix[4]arene (P_1), do not exhibit any gelation, suggesting that both the calixarene platform as well as the cholesteryl moiety together are essential to form the gel in the present case.

The gelation of **G** dissolved in THF by incremental addition of CH_3CN was initially monitored visually (Figure 1a) and later

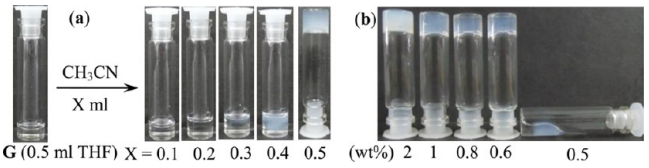

Figure 1. (a) Phase behavior of the system **G** in THF by the addition of different volumes (*X* mL) of CH_3CN. (b) Gels obtained at different wt % of **G**.

by spectroscopy and microscopy as discussed in this paper. The minimum gelator concentration of **G** in THF/CH_3CN (1:1 v/v) is 0.6 wt % (Figure 1b). Other calix conjugates reported in the literature exhibited minimum gelator concentration of 1 wt % for bisamide-linked dicholesteryl-calix[4]arene, <2 wt % for 9,10-bisisoxazolylanthracenebiscalix[4]arene and 0.05−0.13 wt % for thienyl-2,5-bisisoxazolyl-methylbiscalix[4]arene.[37−39] The gel formation was observed even up to 5 wt % system in the present case. However, 1 wt % gel was used for all the studies reported throughout the paper.

Characterization of the Gel. The 1 wt % gel obtained from THF/CH_3CN (1:1 v/v) has been characterized by spectroscopy and microscopy. The absorption spectra recorded for **G** in THF solution showed a band at 298 nm corresponding to $\pi \rightarrow \pi^*$ transition from the aromatic groups of the calixarene platform. However, upon gelation this band is broadened, and a new shoulder appears at 320 nm whose absorbance increases as the added volume of CH_3CN increases (Figure 2a). The new band observed at 320 nm is attributable to the formation of J-aggregates. In case of J-aggregates, the molecules tend to arrange themselves in lateral or slipped fashion under a suitable solvent medium.[46,47] The **G** exhibits emission at 317 nm (λ_{ex} = 285 nm) with an increase almost by 600% (Figure 2b) in the corresponding gel due to aggregation-induced enhancement (AIE).[48−50]

The SEM images taken for **G** in sol showed aggregates of nanospheres of ∼100 nm size, while that of the gel shows orderly arranged bundles of nanowires of several microns length and 60 to 70 nm in diameter (Figure 2c−e). A keen observation of these bundles reveals that most of these are twisted or intertwined structures having a diameter of 15−20 nm. It is also noticed that the length and diameter of these

DOI: 10.1021/acsami.5b02506
ACS Appl. Mater. Interfaces 2015, 7, 11555−11566

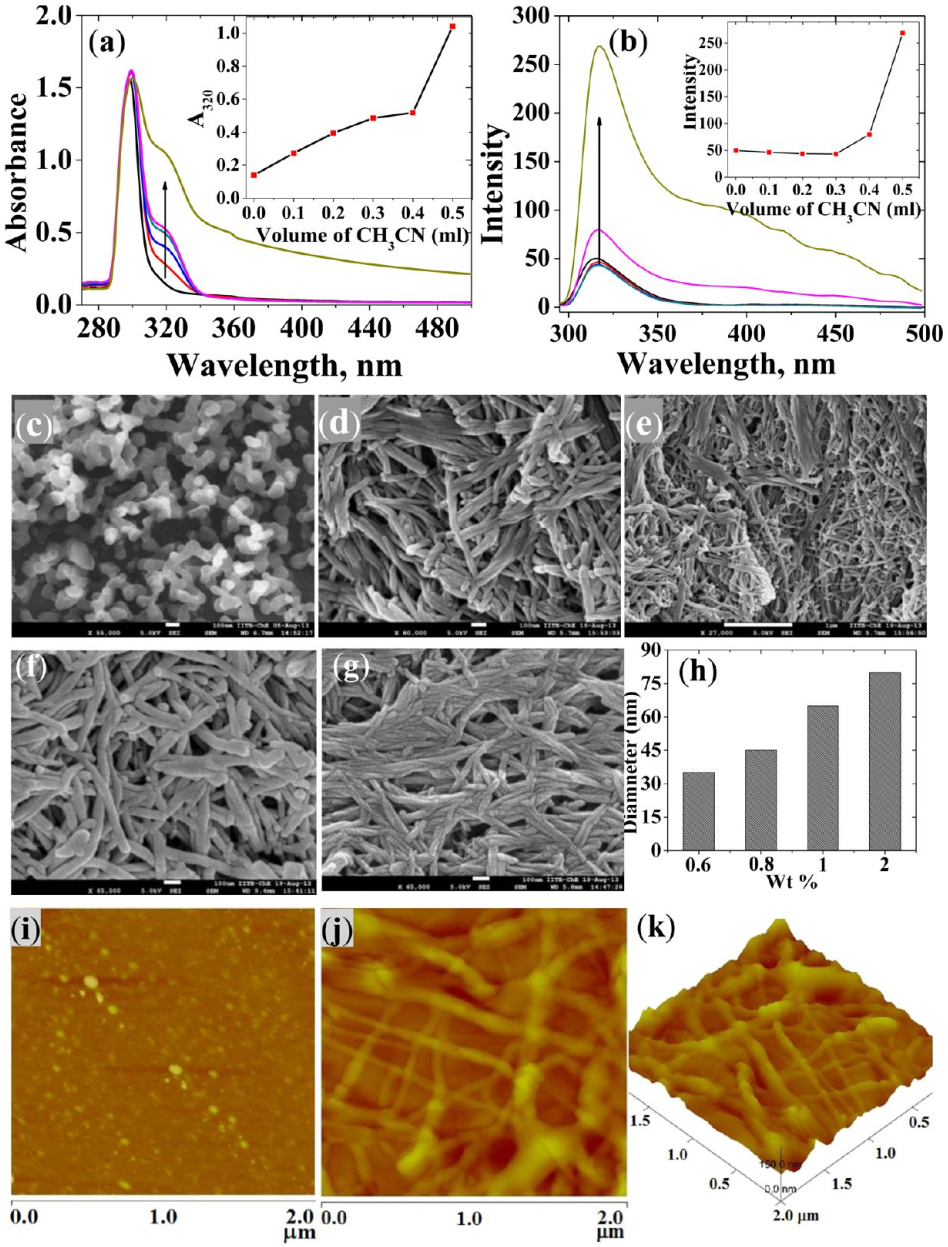

Figure 2. (a) Absorption spectra measured during the formation of gel upon addition of different volumes (mL) of CH_3CN to **G** taken in THF. Inset: plot of absorbance at 320 nm vs volume of CH_3CN added. (b) Fluorescence spectra measured during the formation of gel upon addition of different volumes of CH_3CN to **G** taken in THF. Inset: plot of emission at 317 nm vs volume of CH_3CN added. (c–g) SEM images: (c) **G** in THF as sol; (d) and (e) for the gel (1 wt %) at 100 nm and 1 μm scale bar; (f) and (g) for 2 and 0.6 wt % gel, respectively. (h) Bar diagram for the diameter (nm) vs wt % of the gel. (i–k) AFM images: (i) **G** in THF as sol; (j) and (k) for the gel in 2D and 3D view.

nanobundles increases with increasing concentration of the gelator, and the diameter changes from 30 to ~80 nm on going from 0.6 to 2.0 wt % (Figure 2f–h). In AFM, the **G** in sol forms very thin aggregated nanostructures of 10–15 nm (Figure 2i) height. That of the gel forms a network of nanobundles with the length running to a few microns and the diameter to 70–90 nm, while the height varies from 15 to 30 nm (Figure 2j,k). Thus, both the SEM and AFM support bundle-like structures which are twisted, intertwined, and branched for the gel.

In fact, the present gelator system (**G**) is unique as compared to bischolesteryl-functionalized calix[4]arene systems reported recently.[41,42] This is due to the fact that **G** is monofunctionalized and results in instantaneous gelation for a variety of solvent combinations at low CGC. However, the reported bischolesteryl functionalized calix[4]arene systems form gel upon agitation or sonication in limited solvent systems and comparatively high CGC (1 to 2.5 wt %). In addition, in the present case the gel showed a long and intertwined bundle-like network as observed from both the AFM and SEM (Figure 2) representing the degree and ease of self-assembly. Such intertwined bundle-like network structures helps in storing drug molecules as reported later in this paper.

Molecular Modeling of Gel. In order to understand self-assembly of gelator molecules, the DFT and MM computational studies were carried out. The monomer unit, **G**, was optimized (Figure 3a) using the DFT level of computation as mentioned in the Experimental Section. The optimized **G** was used for making a dimer $\mathbf{G}_2$ by bringing two **G** units either in a

DOI: 10.1021/acsami.5b02506
ACS Appl. Mater. Interfaces 2015, 7, 11555–11566

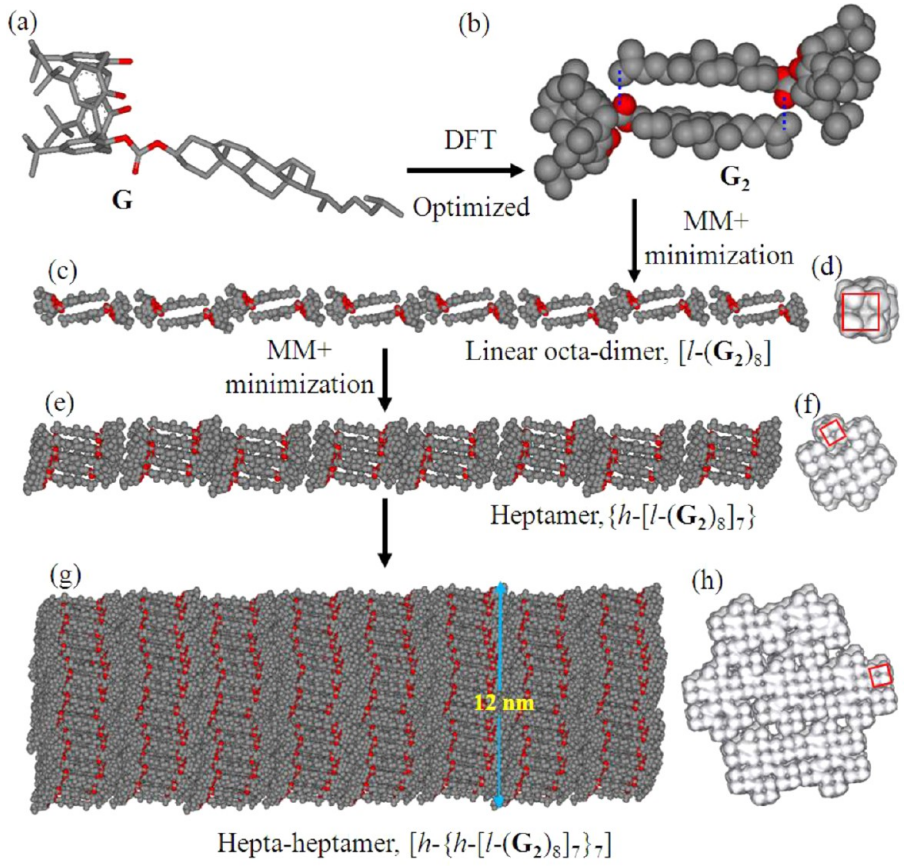

Figure 3. Flowchart showing the steps involved in the molecular modeling of $[h\text{-}\{h\text{-}[l\text{-}(\mathbf{G}_2)_8]_7\}_7]$: the DFT optimized structures for (a) **G** and (b) $\mathbf{G}_2$. MM minimized structures: (c) linear octadimer, $[l\text{-}(\mathbf{G}_2)_8]$. (d) The view perpendicular to the propagation axis in $[l\text{-}(\mathbf{G}_2)_8]$. (e) heptamer of the linear octadimer (simply referred to as "heptamer"), $\{h\text{-}[l\text{-}(\mathbf{G}_2)_8]_7\}$. (f) The view perpendicular to the propagation axis of $\{h\text{-}[l\text{-}(\mathbf{G}_2)_8]_7\}$. (g) "Heptamer of the heptamer", $[h\text{-}\{h\text{-}[l\text{-}(\mathbf{G}_2)_8]_7\}_7]$. (h) The view perpendicular to the propagation axis of $[h\text{-}\{h\text{-}[l\text{-}(\mathbf{G}_2)_8]_7\}_7]$. The red square denotes the cavity of the calix[4]arene.

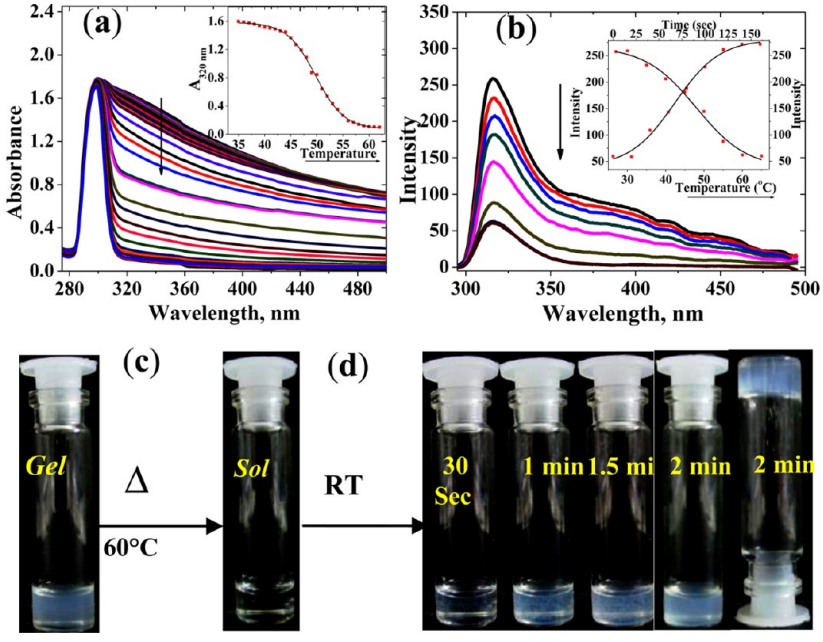

Figure 4. (a) Absorption spectra measured by varying the temperature to bring gel → sol transition. Inset is a plot of absorbance at 325 nm vs temperature. (b) Fluorescence spectra measured by varying the temperature to bring the gel → sol transition. Inset is a plot of intensity vs temperature and time vs temperature. Photographic images: (c) gel → sol and (d) $\text{sol}_{(\text{hot})}$ → gel (as a function of time) transition.

DOI: 10.1021/acsami.5b02506
ACS Appl. Mater. Interfaces 2015, 7, 11555−11566

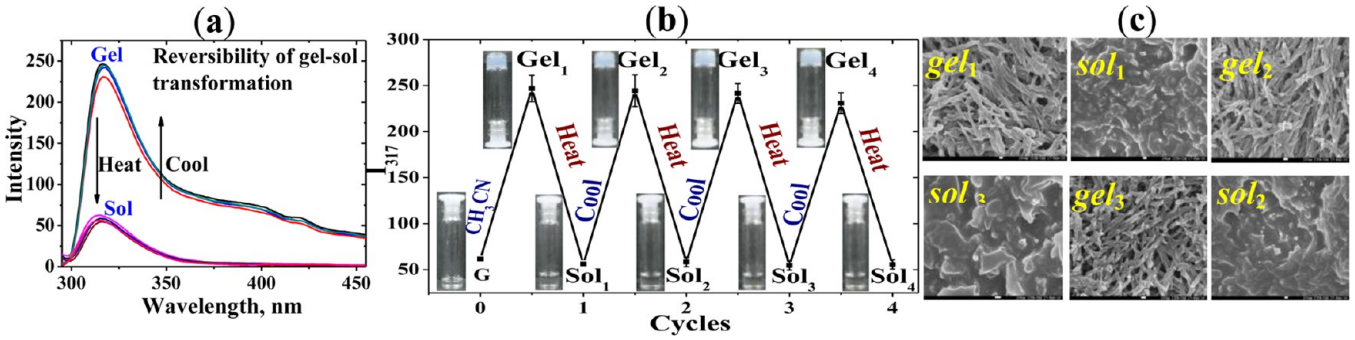

Figure 5. (a) Fluorescence spectra for the reversibility of gel ↔ sol transformation shown for four cycles. (b) Photograph of vials corresponding to that in (a) for all the four cycles. (c) SEM images for the reversibility of gel ↔ sol transformation (shown for three cycles).

head-to-head or in a head-to-tail fashion. When computation was carried out in a head-to-head fashion, the optimization process resulted in a dimeric structure where the cholesteryl parts of the two molecules go farther apart leaving very little cohesive interaction between both the **G**'s. This is clearly due to the approach of the tertiary butyl groups present on the upper rim of both the gelator molecules. On the other hand, the dimer optimized in a head-to-tail fashion resulted in a structure in which the cholesteryl units pack better and are also well stabilized. The complexation stabilization energy calculations support the dimer that is formed in head-to-tail arrangement by 13.9 kcal/mol as compared to the head-to-head dimer. Therefore, the head-to-tail dimer was used in all the computational studies.

In the $\mathbf{G}_2$, each **G** exhibits a C−H···O hydrogen bond at the terminal (C−H) of one of the cholesteryl units with "O" of C═O of the second cholesteryl moiety and vice versa. These hydrogen bonds, viz., C−H···O (D···A = 3.56, 3.55 Å, H···A = 2.48, 2.47 Å, and ∠D-H···A = 173.1, 174.5°) are responsible for stabilizing the dimer, $\mathbf{G}_2$. In order to achieve an extended structure, eight such dimeric units are brought nearer linearly by placing each $\mathbf{G}_2$ unit in an end-to-end fashion and then used for the minimization.

Thus, the energy-minimized linear octamer, $[l\text{-}(\mathbf{G}_2)_8]$ (Figure 3c), contains eight $\mathbf{G}_2$ units in which the upper rim of one of the $\mathbf{G}_2$ unit faces the upper rim of second $\mathbf{G}_2$, and this is extended throughout the octamer species. The length of the octamer is ∼30 nm, and the diameter is ∼1.4 nm. These can further self-assemble. It was well explored in the literature that an appropriate balance of attractive and repulsive forces among molecular scaffolds could mediate the formation of supramolecular structures.[51] One such possible arrangement that leads to a symmetrical and cylindrical structures has hexagonal-type packing. Thus, a heptamer is built by using six $[l\text{-}(\mathbf{G}_2)_8]$ around the central one in a hexagon fashion as shown in Figure 3e, and the energies were minimized. In the energy-minimized structure, the diameter of the hexagonal heptamer, $\{h\text{-}[l\text{-}(\mathbf{G}_2)_8]_7\}$, is 3.8 nm. Finally, in order to obtain a cylindrical bundle, a heptamer of these heptamers, $[h\text{-}\{h\text{-}[l\text{-}(\mathbf{G}_2)_8]_7\}_7]$ (Figure 3g), was constructed by going through a similar exercise as that of the former step. The diameter of this bundle is ∼12 nm which is comparable to the diameter of some of the bundles observed from the SEM studies.

Gel ↔ Sol Transitions. The gel looks fresh and intact even after two months when it is stored in a tightly closed vial that is kept in a refrigerator, reflecting on the long-term stability of the gel. On the other hand, when the gels are left at room temperature in closed vials, these turned powdery due to the loss of solvent over a period of one month (Figure S4, Supporting Information). The gel transforms to sol when heated to 60 °C (Figure 4c) and returns back to gel upon cooling to room temperature within 2 min (Figure 4d), supporting the thermoreversibility of the gel.

A variable-temperature absorption experiment carried out for the gel−sol transition (Figure 4a) revealed that upon increasing the temperature the broad band corresponding to the j-aggregates of the gel decreases gradually, and at ∼60 °C this band is vanished completely, indicating the collapse of the gel yielding sol. A plot drawn for the absorbance at 325 nm vs temperature gave a sigmoidal curve with an inflection point centered at 49 ± 1 °C. Similar studies were carried out by emission spectroscopy and found a sigmoidal curve with $T_{\text{gel}\rightarrow\text{sol}}$ at 48 ± 1 °C as shown in Figure 4b.

The sol → gel is demonstrated by measuring the fluorescence emission while cooling the hot sol obtained at 60 °C over a period of 2 min where the measurement is taken after every 20 s. The gelation starts after leaving the hot sol unheated for 20 s as can be noticed visually (Figure 4d). The fluorescence spectra of the gel thus obtained is the same as that observed for the gel formed by **G** in THF upon addition of acetonitrile (Figure S5, Supporting Information).

Reversibility. A material can be functional if the reversibility behavior can be repeated over several cycles. Thus, in the present case the gel ↔ sol reversibility is achieved several times by carrying out studies in a cyclic fashion as shown in Figure 5 and hence is interesting from the functional point of view, such as storage and release of guests and/or drugs. The reversibility was monitored visually as well by fluorescence and SEM. The emission intensity at 316 nm is enhanced by almost 500% when sol turns to gel.

In SEM studies, the images obtained for the gel_1 show bundles of nanotubes running several microns in length and 80−100 nm in diameter. However, the images obtained for the sol_1 (Figure 5c) showed nanoaggregates of size 50−100 nm. The gel_2 also showed bundles except that they are smaller and shorter as compared to the gel_1, with 70−90 nm diameter. The SEM carried out for $\text{gel}_2 \rightarrow \text{sol}_2$ and $\text{gel}_3 \rightarrow \text{sol}_3$ exhibited similar results. The images obtained for the sol_2 (by heating the gel_2) showed features similar to that of sol_1. The gel_3 (by cooling the sol_2) showed bundles with a smaller diameter (65−85 nm) than that of the gel_2. Finally the sol_3 showed nanoaggregates of different sizes. However, the diameter of the bundles goes from 80 to 100 to 70−90 to 65−85 nm, indicating a marginal level of thinning of bundles by repeating the gel−sol cycles (Figure 5).

DOI: 10.1021/acsami.5b02506
ACS Appl. Mater. Interfaces 2015, 7, 11555−11566

Entrapment of Guests by the Gel. One of the important applications of gels is drug delivery of which the basic requirement for the gel is to encapsulate the drug first and then to release. In order to demonstrate this, the ability of the gel to entrap the guest species was addressed. In the present study, simple organic dyes (*viz.*, brilliant blue and bromophenol blue), common fluorescent molecules (*viz.*, fluorescein, rhodamine), and drugs (*viz.*, doxorubicin, curcumin, and tocopheryl acetate) were used as guest molecules. In all the cases, the guest entrapped gels exhibited color except in the case of tocopheryl acetate where the color of the gel is from that of the guest being entrapped, and these are emissive under UV lamp (Figure 6a–c). The entrapment of the guest molecule in the hydrophobic pockets formed between gelator units in the gel has been monitored by fluorescence spectroscopy, and the possible interactions of these guests within the hydrophobic cavity were modeled computationally.

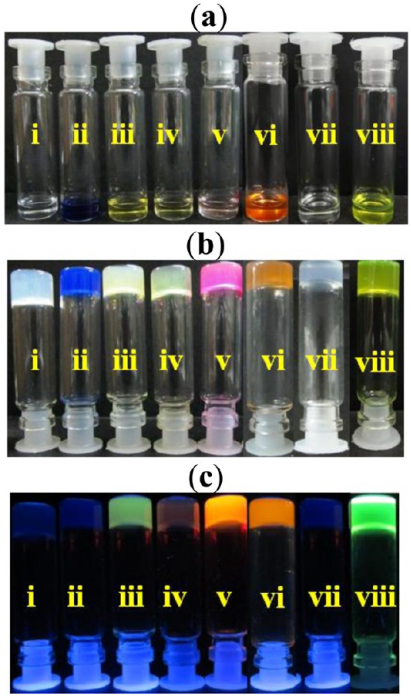

Figure 6. Photographs of colors of vials: {i} is **G** in THF; {ii} is (i) + brilliant blue; {iii} is (i) + fluorescein; {iv} is (i) + bromophenol blue; {v} is (i) + rhodamine; {vi} is (i) + doxorubicin; {vii} is (i) + tocopheryl acetate; {viii} is (i) + curcumin. (a) in solution state; (b) as gels under visible light; (c) the same gels under a 365 nm UV lamp.

Fluorescence Emission of the Guest Entrapped Gels. Fluorescence studies were carried out for the guest-entrapped gels by monitoring the emission of the **G** or the guest or both. For example, while monitoring the emission of rhodamine-entrapped (λ_{ex} = 285 nm) gel, the emission of the **G** at 315 nm is overlapped by the emission arising from the free rhodamine. As the gelation grows, a new broad band (350–500 nm) corresponding to the energy transfer from the excited state of **G** to the entrapped rhodamine was observed (Figure 7a). However, when rhodamine is excited at 440 nm, a new emission band is observed at 585 nm, and its intensity increases at the expense of the 525 nm band (Figure 7b). The enhancement observed at 585 nm is due to the trapped rhodamine in the hydrophobic pockets. Similar spectral changes were observed even in the case of fluorescein-entrapped gel. In the case of fluorescein, when **G** is excited at 285 nm, the fluorescence emission of the new bands that appeared at 325 and 385 nm enhances as the gelation grows (Figure 7c). In the same system, when fluorescein is excited at 450 nm, the emission band at 520 nm increases in its intensity gradually as a result of the gelation (Figure 7d). In all these experiments the fluorescence enhancement results from the entrapment of the guest species in the hydrophobic cavity arising from the **G** in the gel.

In the case of doxorubicin as guest, as the gelation proceeds, the emission bands of doxorubicin (λ_{ex} = 515 nm) observed at 550, 590, and 640 nm exhibit fluorescence enhancement (Figure S6, Supporting Information). In the case of curcumin as guest, as the gelation progresses, the emission band of curcumin (λ_{ex} = 440 nm) observed at 505 nm enhances in intensity with a red shift of ~10 nm (Figure 7e). These spectral changes are suggestive of curcumin being trapped in the hydrophobic pockets of the gel. Marginal changes were also observed in the spectra of **G** during the gelation due to the entrapment of the guest molecule (Figure S6, Supporting Information). In the case of tocopheryl ester as guest, fluorescence could not be monitored as this species does not emit.

Microscopy Features of the Guest-Entrapped Gels. The microscopy features of the guest-entrapped gels were examined by both SEM and AFM as given in Figure 8. From SEM studies, it is noticed that the texture of the gel differs from the simple gel to that of the guest-entrapped one. The nanobundles obtained from the simple gel appear to be smooth and cylindrical, whereas the gels of the guest-entrapped ones appear to be slightly coarse in their texture. The SEM recorded for rhodamine-entrapped gel shows nanobundles of diameter ~30 nm which are further joined and intertwined to give bundles of size 45–60 nm (Figure 8b).

The AFM for this gel showed bundles of diameter 30–60 nm (Figure 8c) with a height of ~10 nm. The SEM for the sol containing rhodamine as a control resulted in spherical particles

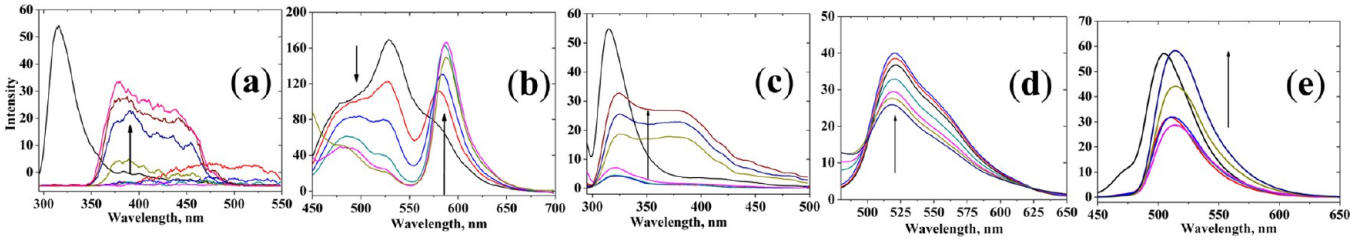

Figure 7. Fluorescence spectra obtained during the entrapment of the guest: (a) rhodamine, λ_{ex} = 285 nm; (b) rhodamine, λ_{ex} = 440 nm; (c) fluorescein, λ_{ex} = 285 nm; (d) fluorescein, λ_{ex} = 450 nm; (e) curcumin, λ_{ex} = 440 nm.

DOI: 10.1021/acsami.5b02506
ACS Appl. Mater. Interfaces 2015, 7, 11555–11566

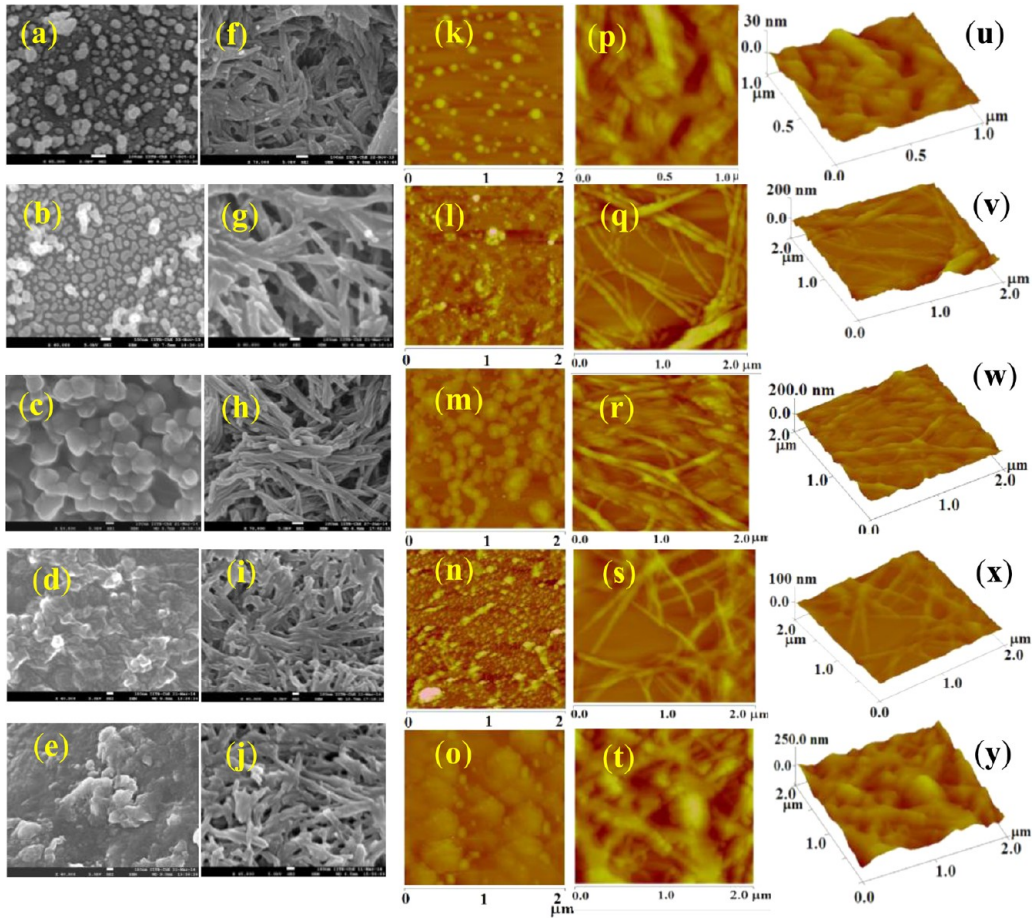

Figure 8. SEM micrographs: (a) to (e) are in the sol state along with the guest species, and (f) to (j) are the gels where the guest is entrapped. AFM micrographs: (k) to (o) are in the sol state along with the guest species, and (p) to (t) are the gels where the guest is entrapped. From (u) to (y) are the AFM micrographs (as 3D) in the gels where the guest is entrapped. The guest species from top to bottom: row 1 is rhodamine; row 2 is fluorescein; row 3 is doxorubicin; row 4 is curcumin; and row 5 is tocopheryl acetate. All these are entrapped in the gel.

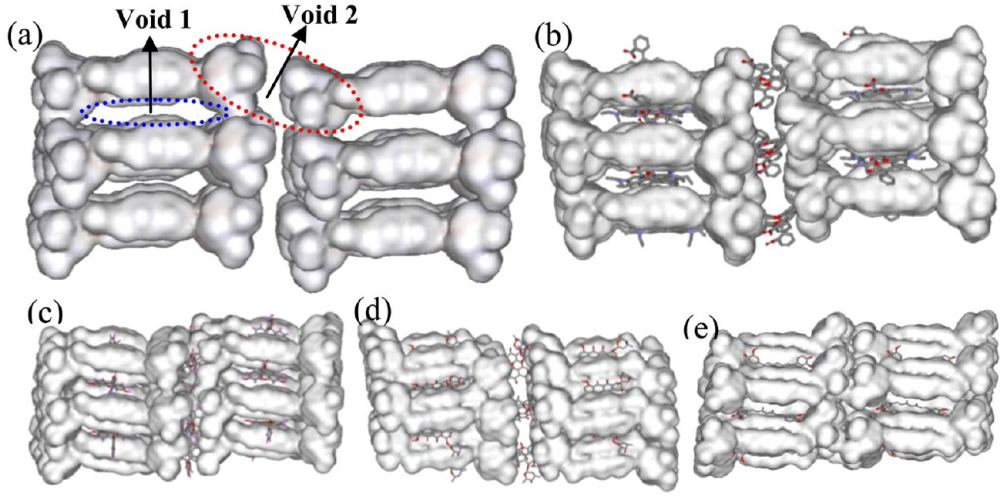

Figure 9. (a) Surface representation form of truncated heptadimer, $\{[(G_2)_7]_2\}$. The guest-entrapped heptadimer: (b) rhodamine; (c) fluorescein; (d) doxorubicin; (e) curcumin.

of size 25−40 nm, and some of these are joined together to give large size aggregates of 100−150 nm (Figure 8a). Similar microfeatures were observed for rhodamine even in AFM (Figure 8k). The SEM recorded for fluorescein-entrapped gel shows bundles of size 50−60 nm in diameter, while the length is several microns (Figure 8g). The same under AFM (Figure 8q,v) shows that the height of these bundles is 15−20 nm. The sol containing fluorescein as a control yielded spherical aggregates of varying sizes in SEM (Figure 8d) and AFM (Figure 8l). In the case of doxorubicin-entrapped gel, it is observed from SEM that the features of this gel are marginally different from that of all other gels in their morphology.

DOI: 10.1021/acsami.5b02506
ACS Appl. Mater. Interfaces 2015, 7, 11555−11566

Uniform tube like structures of size ~20 nm are joined and intertwined, yielding large size bundles of 35−120 nm in diameter (Figure 8h). The height of these bundles is 10−25 nm as observed from AFM (Figure 8r,w). In the case of sol containing doxorubicin as a control, uniform aggregated spherical particles of size 100−200 nm were observed in both SEM (Figure 8g) and AFM (Figure 8m).

However, SEM recorded for curcumin-entrapped gel showed a network of nanobundles which appear to be more connected and/or joined with a diameter of 50−80 nm (Figure 8i). The same sample shows a height of 10−20 nm from AFM (Figure 8s,x). The sol containing curcumin alone shows spherical aggregates of ~100 nm in both SEM (Figure 8d) and AFM (Figure 8n). The tocopheryl acetate-entrapped gel also shows nanofeatures similar to that of curcumin with the size of the bundles being 40−50 nm in diameter, and these are further aggregated to give bundles of varying sizes (Figure 8j). These exhibited a height of 15−20 nm in AFM (Figure 8t,y). The microscopy images obtained for sol containing tocopheryl acetate alone showed lump-like features (Figure 8e,o). Thus, the microscopy studies reveal that the guest-entrapped gels have different morphological and structural features as compared to the simple gel as well as the solutions containing guest molecular systems.

Modeling the Guest Entrapment. In order to understand and visualize the interactions present between the guest and the gelator molecules in the gel, the energy-minimized gel structure was filled with guest molecules in their hydrophobic regions, and MM computations were carried out. A truncated heptadimer, viz., $\{[(\mathbf{G}_2)_7]_2\}$, was made from the $\{h\text{-}[l\text{-}(\mathbf{G}_2)_8]_7\}$ (Figure 3e) and was used as model for the gel for the entrapment studies in order to decrease the computational times. The $\{[(\mathbf{G}_2)_7]_2\}$ has hydrophobic void space, viz., "Void 1" and "Void 2", as can be noticed from Figure 9a. Both the "Void 1" and "Void 2" were filled with the corresponding guest species (viz., doxorubicin, curcumin, fluorescein, and rhodamine), and the resultant systems were subjected to energy minimization.

In the minimized structure, the guests, viz., doxorubicin, curcumin, fluorescein, and rhodamine, were entrapped very well in the gel, and the same can be noticed from Figures 9b−e. The guest molecule shows C−H···π interaction through the π system of the guest with C−H of the cholesteryl moiety with a C···π distance of 3.7−4.7 Å (Figure S7, Supporting Information) and hence is responsible for its stability. While all the guest species could be accommodated in "Void 2", the curcumin units could not be placed due to their bulky nature.

$T_{gel\rightarrow sol}$ of Entrapped Guests. From the fluorescence experiments carried out in the temperature 35−75 °C, it is noticed that the guest-entrapped gel−sol transition temperature is 55, 56, 55, 55, and 52 °C, respectively, for rhodamine, fluorescein, doxorubicin, curcumin, and tocopheryl acetate (Figure 10a). Thus, the $T_{gel\rightarrow sol}$ increases from ~48 to ~55 °C, ongoing from the simple gel to the guest-entrapped gels (Figure 10a). The raise in $T_{gel\rightarrow sol}$ is expected because the guest-entrapped gels are relatively more stable than the simple ones.[45] The SEM features clearly show the reproducibility of sol and gel during the transitions (Figure 10b−e). In view of the practical applications of these gels, release of the guest was also studied.

Release of the Guest (Drug) Species. The release of the guest from the gels has been schematically depicted in Figure 11a. To the 1 wt % guest-entrapped gels was slowly added 0.5 mL of water using a micro pipet. While the water settles down, the guest molecules present in the gel are extracted into water leaving the gel network undisturbed (Figure 11b) except in the case of tocopheryl ester-entrapped gel. As the time progresses, more and more of the guest molecules were released into the aqueous phase, and this process was monitored for 2 h.

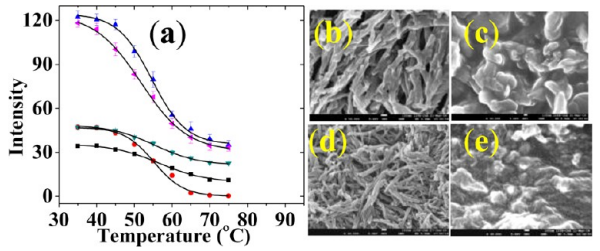

Figure 10. (a) Plot of fluorescein intensity vs temperature carried out for the release of trapped guests: -●, rhodamine; -■, fluorescein; -▼, curcumin; -◀, tocopheryl acetate; -▲, doxorubicin. SEM images of the fluourescein-trapped gel: (b) before and (c) after heating. SEM images of the doxorubicin-trapped gel: (d) before and (e) after heating.

At the end of 2 h, the total amount of guests released into the aqueous medium was estimated by recording their absorption spectra. Thus, the amount of guest (drug) released into the aqueous medium is 92−98% for all the guests studied suggesting an efficient extraction of the guest trapped in the gel into the aqueous medium. The gel material is recovered, and the SEM of the gel after extraction of the guest into aqueous medium showed a microstructure the same as that of the simple gel. This is true in the case of all five guest species (Figure 11c−f), supporting that the structure of the gel network is retained even after extrusion of the guest species from the gel.

Reusability of the Gel for Repeated Cycles of Guest (Drug) Storage Followed by Release. After the release of the guest (drug) species into an aqueous medium, the recovered gel material has been subjected to a second cycle of entrapment and release. This exercise has been done in the case of a drug and a dye species, viz., doxorubicin- and fluorescein-entrapped gels, and was repeated for four cycles. The SEM of the gel was measured after each cycle of extraction of the guest species in order to examine the morphology of the gel, and it was found that the morphology is intact by displaying the structures with twinned bundles of fibrils after every cycle of entrapment and release of the guest species (Figure 12). All this suggests that the gel is a functional material and is reusable for multiple usages of guest storage and release.

■ CONCLUSIONS AND CORRELATIONS

A new cholesteryl monoderivatized calix[4]arene (gelator, **G**) has been synthesized and characterized. The possibility of gelation has been checked in 20 common organic solvents, among which the gelator exhibited remarkable and versatile gelation behavior with various solvent combinations. The minimum gelator concentration of **G** in THF/acetonitrile (1:1 v/v) was found to be 0.6 wt %. In the absorption measurement, as the gelation progresses upon addition of CH_3CN, a new band at ~320 nm appears which corresponds to j-aggregation, while the increase in emission is due to AIE. SEM and AFM images taken for the gel showed a well-organized network of nanobundles, while that of the sol showed spherical nano-aggregates. From the SEM studies, it was noticed that, as the concentration of **G** increases, the length and diameter of the

DOI: 10.1021/acsami.5b02506
ACS Appl. Mater. Interfaces 2015, 7, 11555−11566

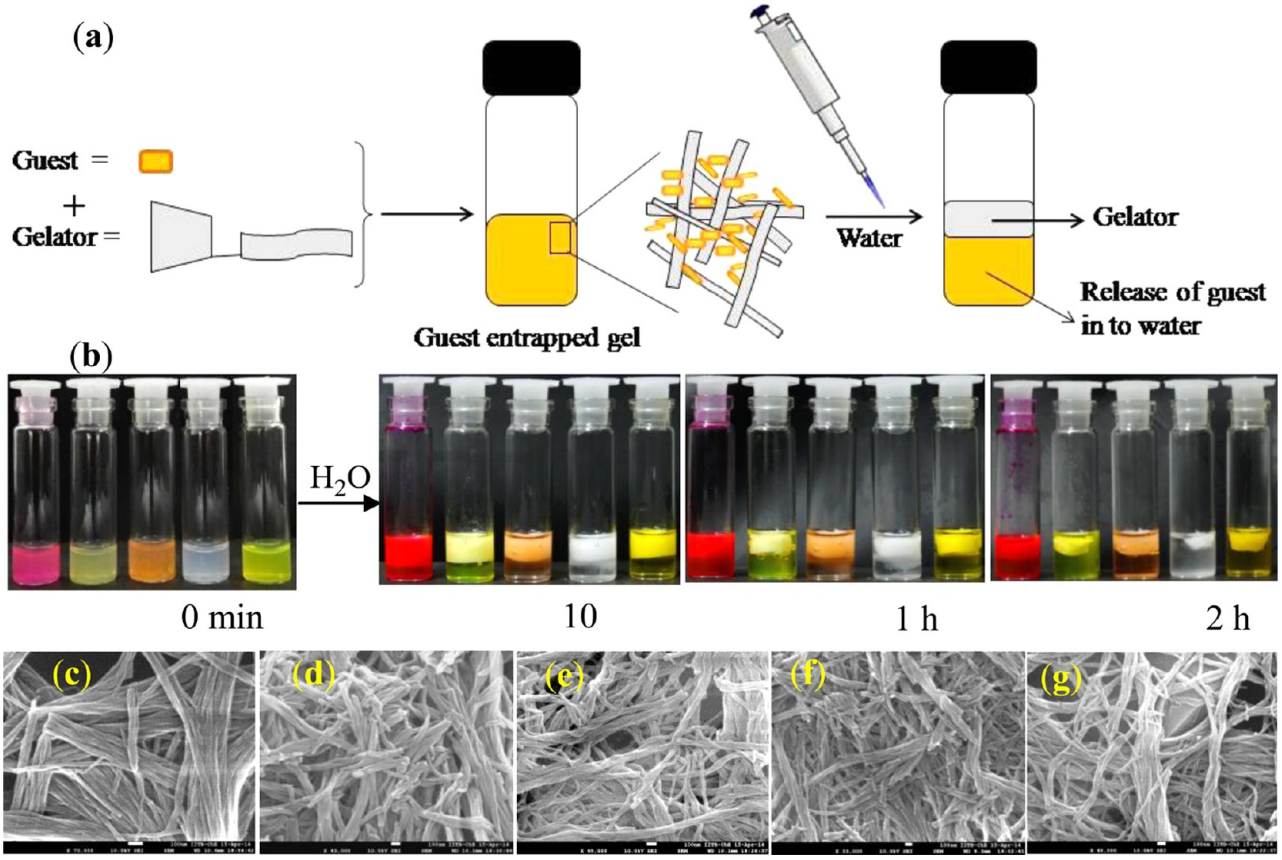

Figure 11. (a) Schematic representation of the water-mediated guest release. (b) Images of the vials of guest-entrapped organogels before and after addition of 0.5 mL of water at different time intervals. SEM of the gelator after extraction of the guest into water from the guest (c) rhodamine, (d) fluorescein, (e) doxorubicin, (f) curcumin, and (g) tocopheryl acetate entrapped gels.

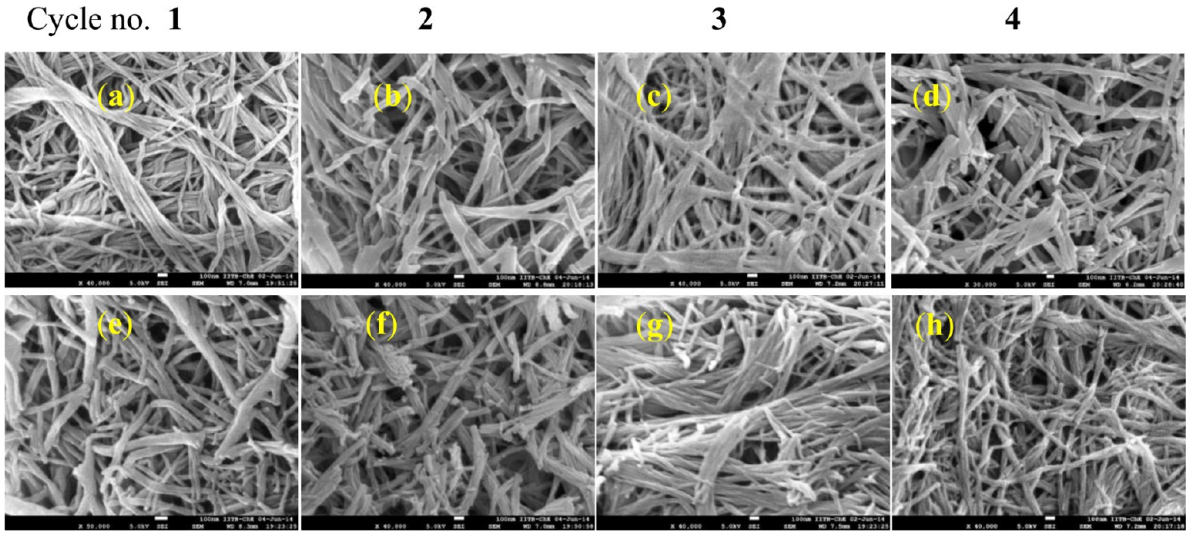

Figure 12. SEM images taken for the gel after release of the guests into water for four consecutive cycles (left to right corresponds cycles 1 to 4, respectively): (a)−(d) are the images for the fluorescein-entrapped gel. (e)−(h) are the images for the doxorubicin-entrapped gel.

bundles formed in the gel also increase (Figure 2h). Amid, the gel showed excellent thermoreversibility. The gel to sol transition ($T_{gel \rightarrow sol}$) occurred at ∼48 °C, whereas the corresponding hot sol turned back to gel when allowed to cool to room temperature. The gel → sol transformation has been achieved for various cycles showing its reversibility.

Computationally modeled assembly of the gelator system yielded a bundle of ∼12 nm diameter with various hydrophobic pockets within. In SEM, the nanobundles obtained from the simple gel appeared to be smooth and cylindrical, whereas the gels of the guest-entrapped ones appeared to be coarse in their texture and differed from the simple gel in their sizes as well. The diameter of bundles in the simple gel is 60−70 nm, while it is marginally contracted to 45−60, 50−60, 35−60, 50−80, and 40−50 nm, respectively, when entrapped by rhodamine, fluourescein, doxorubicin, curcumin, and tocopheryl acetate,

DOI: 10.1021/acsami.5b02506
ACS Appl. Mater. Interfaces 2015, 7, 11555−11566

indicating that the bundles are stabilized in the presence of the guest species which was further supported by the computational study. The detailed fluorescence measurements clearly supported the entrapment of the guest (drug) species in the gel. The modeling study revealed that the possible interactions are between π systems of guest with C−H of the cholesteryl moiety indicating that the trapped guest molecules are stabilized through C−H···π interactions.

All the guest-entrapped gels are stable, and their $T_{gel\rightarrow sol}$ increases by ∼5−7 °C. Thus, the trapped guests were easily released by heating these to the temperatures above RT. Extraction of guest (drug) species into an aqueous medium has been achieved to an extent of 92−98% in about 2 h. Thus, a reversible gel reported in this paper is a functional material which possesses hydrophobic voids and is important in its drug delivery applications and further is reusable for several cycles of storage followed by release of drugs.

EXPERIMENTAL SECTION

^{1}H and ^{13}C NMR spectra were measured on a 400 MHz NMR spectrometer. The mass spectra were recorded on a Q-TOF instrument using the electrospray (ES) ionization method in negative ion mode. Fluorescence and absorption studies were carried out in 1 cm quartz cells with HPLC grade solvents on a PerkinElmer LS55 fluorescence spectrometer and Shimadzu, UV-2101PC UV−vis scanning spectrophotometer, respectively. In all the titrations, the bulk concentration of the gelator (**G**) was kept at 1.8×10^{-2} M in THF. In order to study the gelation, 500 μL of stock solution of **G** in THF was taken each time, and this was added 100−500 μL of CH_3CN gradually. For all the AFM studies carried out on a Bruker digital multimode AFM, 5.6 mM concentration of **G** (**G** + guest) and guest solutions were used. Before drop casting, the solutions were sonicated for 10 min. For all the SEM studies carried out on JEOL FEG-SEM, 1 wt % gel was used except when recording 2, 0.8, and 0.6 wt % gels. The cuvette concentration of **G** is 9.4×10^{-3} M in all its studies with the guest species.

Synthesis and Characterization of the Gelator Molecule (G). The gelator molecule has been synthesized in one step from *p-tert*-butyl calix[4]arene (P_1). To a mixture of P_1 (2 g, 3.08 mmol) in 150 mL of dry acetone, K_2CO_3 (0.85 g, 6.163 mmol), NaI (0.925 g, 6.163 mmol), and cholesteryl chloroformate (2.75 g, 6.163 mmol) were added with stirring and then refluxed for 1 day. The reaction mixture was cooled to room temperature and filtered to get the white crude solid product. The product was again stirred with 100 mL of acetone to dissolve and remove excess cholesteryl chloroformate. The solvent was filtered off, and the product was washed several times with water and was then extracted into 100 mL of CH_2Cl_2. The CH_2Cl_2 layer was washed thrice with 30 mL of water each time, and the water layers were discarded. The CH_2Cl_2 layer was evaporated to obtain pure product of **G** and was characterized by spectroscopy (S1, Supporting Information). Yield (2.51 g, 76%). ^{1}H NMR (400 MHz, $CDCl_3$, δ ppm): 6.9 (m, 6H, Ar−*H*), 6.0 (s, 1H, Ar−*H*), 5.9 (s, 1H, Ar−*H*), 5.4 (t, 1H, C═C*H*), 4.7 (br, 1H, OC*H*), 4.3, 4.2, 3.9 (3d, 8H, Ar−C*H*$_2$−Ar), 3.3 to 0.7 (79H, cholesteryl and *t*-butyl). ^{13}C NMR (400 MHz, DMSO-d_6) δ = 154.3, 153.2, 150.6, 148.9, 147.63, 143.9, 142.1, 139.6, 139.3, 128.9, 126.0, 125.3, 124.9, 123.3, 123.1, 122.8, 79.0, 78.8, 57.1, 56.9, 56.3, 50.3, 50.1, 42.5, 39.9, 39.7, 38.2, 37.2, 36.8, 36.3, 36.0, 34.5, 34.0, 32.1, 31.9, 31.7, 31.3, 28.4, 28.2, 27.9, 24.5, 24.0, 23.0, 22.7, 21.7, 21.2, 20.1, 19.4, 18.9, 12.1. ESI-MS (negative ion mode): m/z = 1060 $(M - H)^-$. Anal. Calcd for $C_{72}H_{102}O_7$: C, 81.00; H, 9.52. Found: C, 80.56; H, 9.28. FTIR (cm^{-1}): $\nu_{(O-H)}$ 3568 and 3503, $\nu_{(C-H)}$ 2973 and 2851, $\nu_{(C=O)}$ 1759, $\nu_{(C=C)}$ 1459.

Computational Details. The computational calculations were carried out to model the microstructures observed for the gel. The initial model for **G** and its dimer were achieved through DFT studies, whereas the self-assembly and the guest entrap were carried out using MM calculations. The initial model for **G** was taken from the crystal structure reported by us[52] upon bringing the following modifications: (i) both the 1,3-dinaphthalimide arms were chopped at phenolate oxygens of calix[4]arene, and (ii) the cholesteryl unit is attached to phenolate "O" of calix[4]arene through a carbonate link. The starting input model for the **G** was optimized through DFT using B3LYP/6-31G and was given as the input for the dimer, viz., $\mathbf{G}_2$ computations. The $\mathbf{G}_2$ was made by bringing two **G** units such that both the cholesteryl moieties align one over the other and was optimized through DFT. All the DFT computational calculations of **G** and $\mathbf{G}_2$ were carried out using the Gaussian 03 package[53]

Minimization of Heptamer. In order to build the structure noticed in the gel, molecular mechanics calculations were carried out by bringing eight dimeric units together to form a linear octadimer [*l*-$(\mathbf{G}_2)_8$], and this was minimized using HyperChem software.[54] A heptamer of [*l*-$(\mathbf{G}_2)_8$] was built by keeping six such minimized [*l*-$(\mathbf{G}_2)_8$] units to result in a hexagon with the center being filled with the seventh one, which is denoted as {*h*-[*l*-$(\mathbf{G}_2)_8]_7$}. In order to mimic the cylindrical bundle-like structure that was noticed from SEM, these heptamers of linear octadimers, viz., {*h*-[*l*-$(\mathbf{G}_2)_8]_7$}, were constructed to give 7 × 7 structure similar to that of the former step, and these are denoted as [*h*-{*h*-[*l*-$(\mathbf{G}_2)_8]_7$}$_7$]. Thus, the final 7 × 7 structure is built using 784 (2 × 8 × 7 × 7) gelator molecules.

Minimization of the Guest-Entrapped Heptadimer. In order to understand the possible interactions present between the guest and the gelator, a model for the entrapped gel was made from a fragment of the energy-minimized gel structure, and a dimer of a hepta-dimer, {[$(\mathbf{G}_2)_7]_2$}, was used for doping the guest molecules in their hydrophobic pockets and was used for the MM calculations in order to decrease the computational times since this model uses only 28 gelator molecules. This has been achieved by keeping the hydrophobic part of the guest molecule, viz., doxorubicin, curcumin, fluorescein, and rhodamine, in the void space and subjecting the whole system to energy minimization.

ASSOCIATED CONTENT

Supporting Information

Characterization data of the **G**, gelation aspetcs, fluorescence spectra, AFM data, and Cartesian coordinates for DFT-optimized structure of **G** and $\mathbf{G}_2$. The Supporting Information is available free of charge on the ACS Publications website at DOI: 10.1021/acsami.5b02506.

AUTHOR INFORMATION

Corresponding Author

*Phone: 91 22 2576 7162. Fax: 91 22 2572 3480. E-mail: cprao@iitb.ac.in.

Notes

The authors declare no competing financial interest.

ACKNOWLEDGMENTS

CPR thanks the DST (SERB and Nano mission), CSIR, and BRNS for financial support. AKB and VKH acknowledges CSIR, and YSD acknowledges UGC for their fellowships. We also thank Kushal Samanta for some experimental help. We acknowledge the CRYO-FEG-SEM and SPM facilities of IIT Bombay for SEM and AFM measurements, respectively. We dedicate this paper to our mentor, Professor C.N.R. Rao, FRS.

REFERENCES

(1) Terech, P.; Weiss, R. G. Low Molecular Mass Gelators of Organic Liquids and the Properties of Their Gels. *Chem. Rev.* **1997**, *97*, 3133−3159.

(2) Hirst, A. R.; Escuder, B.; Miravet, J. F.; Smith, D. K. High-Tech Applications of Self-Assembling Supramolecular Nanostructured Gel-Phase Materials: From Regenerative Medicine to Electronic Devices. *Angew.Chem., Int. Ed.* **2008**, *47*, 8002−8018.

DOI: 10.1021/acsami.5b02506
ACS Appl. Mater. Interfaces 2015, 7, 11555−11566

(3) Babu, S. S.; Praveen, V. K.; Ajayaghosh, A. Functional π-Gelators and Their Applications. *Chem. Rev.* **2014**, *114*, 1973−2129.
(4) Estroff, L. A.; Hamilton, A. D. Water Gelation by Small Organic Molecules. *Chem. Rev.* **2004**, *104*, 1201−1218.
(5) Sangeetha, N. M.; Maitra, U. Supramolecular Gels: Functions and Uses. *Chem. Soc. Rev.* **2005**, *34*, 821−836.
(6) Ajayaghosh, A.; Praveen, V. K.; Vijayakumar, C.; George, S. J. Molecular Wire Encapsulated into π-Organogels: Efficient Supramolecular Light-Harvesting Antennae with Color-Tunable Emission. *Angew. Chem.* **2007**, *119*, 6376−6381.
(7) Hou, X.; Gao, D.; Yan, J.; Ma, Y.; Liu, K.; Fang, Y. Novel Dimeric Cholesteryl Derivatives and Their Smart Thixotropic Gels. *Langmuir* **2011**, *27*, 12156−12163.
(8) Steed, J. W. Supramolecular Gel Chemistry: Developments over the last Decade. *Chem. Commun.* **2011**, *47*, 1379−1383.
(9) Strandman, S.; Devedec, F. L.; Zhu, X. X. Self-Assembly of Bile Acid−PEG Conjugates in Aqueous Solutions. *J. Phys. Chem. B* **2013**, *117*, 252−258.
(10) Chen, Q.; Feng, Y.; Zhang, D.; Zhang, G.; Fan, Q.; Sun, S.; Zhu, D. Light-Triggered Self-Assembly of a Spiropyran-Functionalized Dendron into Nano-/Micrometer-Sized Particles and Photoresponsive Organogel with Switchable Fluorescence. *Adv. Funct. Mater.* **2010**, *20*, 36−42.
(11) Das, D.; Dasgupta, A.; Roy, S.; Mitra, R. N.; Debnath, S.; Das, P. K. Water Gelation of an Amino Acid-Based Amphiphile. *Chem.—Eur. J.* **2006**, *12*, 5068−5074.
(12) Hoeben, F. J. M.; Jonkheijm, P.; Meijer, E. W.; Schenning, A. P. H. J. About Supramolecular Assemblies of π-Conjugated Systems. *Chem. Rev.* **2005**, *105*, 1491−1546.
(13) Esch, J. H. V.; Feringa, B. L. New Functional Materials Based on Self-Assembling Organogels: From Serendipity towards Design. *Angew. Chem, Int. Ed.* **2000**, *39*, 2263−2266.
(14) Yang, H.; Yi, T.; Zhou, Z.; Zhou, Y.; Wu, J.; Xu, M.; Li, F.; Huang, C. Switchable Fluorescent Organogels and Mesomorphic Superstructure Based on Naphthalene Derivatives. *Langmuir* **2007**, *23*, 8224−8230.
(15) Mohmeyer, N.; Schmidt, H. W. Synthesis and Structure−Property Relationships of Amphiphilic Organogelators. *Chem.—Eur. J.* **2007**, *13*, 4499−4509.
(16) Tang, S.; Liu, X. Y.; Strom, C. S. Producing Supramolecular Functional Materials Based on Fiber Network Reconstruction. *Adv. Funct. Mater.* **2009**, *19*, 2252−2259.
(17) Cai, W.; Wang, G. T.; Xu, Y. X.; Jiang, X. K.; Li, Z. T. Vesicles and Organogels from Foldamers: A Solvent-Modulated Self-Assembling Process. *J. Am. Chem. Soc.* **2008**, *130*, 6936−6937.
(18) Chung, J. W.; An, B − K.; Park, S. P. A Thermoreversible and Proton-Induced Gel-Sol Phase Transition with Remarkable Fluorescence Variation. *Chem. Mater.* **2008**, *20*, 6750−6755.
(19) Kar, T.; Debnath, S.; Das, D.; Shome, A.; Das, P. K. Organogelation and Hydrogelation of Low-Molecular-Weight Amphiphilic Dipeptides: pH Responsiveness in Phase-Selective Gelation and Dye Removal. *Langmuir* **2009**, *25*, 8639−8648.
(20) Chen, X.; Huang, Z.; Chen, S.-Y.; Li, K.; Yu, X.-Q.; Pu, L. Enantioselective Gel Collapsing: A New Means of Visual Chiral Sensing. *J. Am. Chem. Soc.* **2010**, *132*, 7297−7299.
(21) Wang, C.; Chen, Q.; Sun, F.; Zhang, D.; Zhang, G.; Huang, Y.; Zhao, R.; Zhu, D. Multistimuli Responsive Organogels Based on a New Gelator Featuring Tetrathiafulvalene and Azobenzene Groups: Reversible Tuning of the Gel-Sol Transition by Redox Reactions and Light Irradiation. *J. Am. Chem. Soc.* **2010**, *132*, 3092−3096.
(22) Hirst, A. R.; Escuder, B.; Miravet, J. F.; Smith, D. K. High-Tech Applications of Self-Assembling Supramolecular Nanostructured Gel-Phase Materials: From Regenerative Medicine to Electronic Devices. *Angew. Chem., Int. Ed.* **2008**, *47*, 8002−8018.
(23) Das, D.; Das, R.; Mandal, J.; Ghosh, A.; Pal, S. Dextrin Crosslinked with Poly(Lactic Acid): A Novel Hydrogel for Controlled Drug Release Application. *J. Appl. Polym. Sci.* **2014**, DOI: 10.1002/APP.40039.
(24) Vemula, P. K.; Li, J.; John, G. Enzyme Catalysis: Tool to Make and Break Amygdalin Hydrogelators from Renewable Resources: A Delivery Model for Hydrophobic Drugs. *J. Am. Chem. Soc.* **2006**, *128*, 8932−8938.
(25) Xu, H.; Rudkevich, D. M. Controlling Capture and Release of Guests from Cross-Linked Supramolecular Polymers. *Org. Lett.* **2005**, *7*, 3223−3226.
(26) Zheng, Y. S; Ji, A.; Chen, X. J.; Zhou, J. L. Enantioselective Nanofiber-Spinning of Chiral Calixarene Receptor with Guest. *Chem. Commun.* **2007**, 3398−3400.
(27) George, M.; Weiss, R. G. Molecular Organogels. Soft Matter Comprised of Low-Molecular-Mass Organic Gelators and Organic Liquids. *Acc. Chem. Res.* **2006**, *39*, 489−497.
(28) Chen, Q.; Zhang, D.; Zhang, G.; Zhu, D. New Cholesterol-Based Gelators with Maleimide Unit and the Relevant Michael Adducts: Chemoresponsive Organogels. *Langmuir* **2009**, *25*, 11436−11441.
(29) Banerjee, S.; Das, R. K.; Maitra, U. Supramolecular Gels, "In Action". *J. Mater. Chem.* **2009**, *19*, 6649−6687.
(30) Tomasini, C.; Castellucci, N. Peptides and Peptidomimetics that Behave as Low Molecular Weight Gelators. *Chem. Soc. Rev.* **2013**, *42*, 156−172.
(31) Kotharangannagari, V. K.; Ferrer, A. S.; Ruokolainen, J.; Mezzenga, R. Thermoreversible Gel−Sol Behavior of Rod−Coil−Rod Peptide-Based Triblock Copolymers. *Macromolecules* **2012**, *45*, 1982−1990.
(32) Kuang, G. C.; Jia, X. R.; Teng, M. J.; Chen, E. Q.; Li, W. S.; Ji, Y. Organogels and Liquid Crystalline Properties of Amino Acid-Based Dendrons: A Systematic Study on Structure−Property Relationship. *Chem. Mater.* **2012**, *24*, 71−80.
(33) Shirakawa, M.; Fujita, N.; Shinkai, S. A Stable Single Piece of Unimolecularly π-Stacked Porphyrin Aggregate in a Thixotropic Low Molecular Weight Gel: A One- Dimensional Molecular Template for Polydiacetylene Wiring up to Several Tens of Micrometers in Length. *J. Am. Chem. Soc.* **2005**, *127*, 4164−4165.
(34) Kandpal, M.; Bandela, A. K.; Hinge, V. K.; Rao, V. R.; Rao, C. P. Fluorescence and Piezoresistive Cantilever Sensing of Trinitrotoluene by An Upper Rim Tetra-benzimidazole Conjugate of Calix[4]arene and the Delineation of the Features of the Complex by Molecular Dynamics. *ACS Appl. Mater. Interfaces* **2013**, *5*, 13448−13456.
(35) Aoki, M.; Nakashima, K.; Kawabata, H.; Tsutsui, S.; Shinkai, S. Molecular Design and Characterizations of New Calixarene-based Gelators of Organic Fluids. *J. Chem. Soc., Perkin Trans. 2* **1993**, 347−354.
(36) Goh, C. Y.; Becker, T.; Brown, D. H.; Skelton, B. W.; Jones, F.; Mocerino, M.; Ogden, M. I. Self-inclusion of Proline-Functionalised Calix[4]arene Leads to Hydrogelation. *Chem. Commun.* **2011**, *47*, 6057−6059.
(37) Park, J.; Lee, J. H.; Jaworski, J.; Shinkai, S.; Jung, J. H. Luminescent Calix[4]arene-Based Metallogel Formed at Different Solvent Composition. *Inorg. Chem.* **2014**, *53*, 7181−7187.
(38) Wang, K.; Chen, Y.; Liu, Y. A Polycation-Induced Secondary Assembly of Amphiphilic Calixarene and its Multi-Stimuli Responsive Gelation Behavior. *Chem. Commun.* **2015**, *51*, 1647−1649.
(39) Choi, H.; Lee, J. H.; Jung, J. H. Roles of both Amines and Acid in Supramolecular Hydrogel Formation of Tetracarboxyl Acid Appended Calix[4]arene Gelator. *RSC Adv.* **2015**, *5*, 20066−20072.
(40) Wu, Y.; Liu, K.; Chen, X.; Chen, Y.; Zhang, S.; Peng, J.; Fang, Y. A Novel Calix[4]arene-based Dimeric-Cholesteryl Derivative: Synthesis, Gelation and Unusual Properties. *New J. Chem.* **2015**, *39*, 639−649.
(41) Cai, X.; Liu, K.; Yan, J.; Zhang, H.; Hou, X.; Liua, Z.; Fang, Y. Calix[4]arene-based Supramolecular Gels with Unprecedented Rheological Properties. *Soft Matter* **2012**, *8*, 3756−3761.
(42) Cai, X.; Wu, Y.; Wang, L.; Yan, N.; Liu, J.; Fanga, X.; Fang, Y. Mechano-responsive Calix[4]arene-Based Molecular Gels: Agitation Induced Gelation and Hardening. *Soft Matter* **2013**, *9*, 5807−5814.
(43) Tsai, C. C.; Chang, K. C.; I-Ting Ho, I.-T.; Chu, J. H.; Cheng, Y. T.; Shen, L. C.; Chung, W. S. Evolution of Nano- to Microsized

Spherical Assemblies of Fluorogenic Biscalix[4]arenes into Supramolecular Organogels. *Chem. Commun.* **2013**, *49*, 3037−3039.
(44) Tsai, C. C.; Cheng, Y. T.; Shen, L. C.; Chang, K.-C.; I-Ting Ho, I.-T.; Chu, J. H.; Chung, W. S. Biscalix[4]arene Derivative As a Very Efficient Phase Selective Gelator for Oil Spill Recovery. *Org. Lett.* **2013**, *15*, 5830−5833.
(45) Hongyu, G.; Fafu, Y.; Weiwei, L.; Jianbin, L. Novel Supramolecular Liquid Crystals: Synthesis and Mesomorphic Properties of Calix[4]Arene-Cholesterol Derivatives. *Tetrahedron Lett.* **2015**, *56*, 866−870.
(46) Okada, S.; Segawa, H. Substituent-Control Exciton in J-Aggregates of Protonated Water-Insoluble Porphyrins. *J. Am. Chem. Soc.* **2003**, *125*, 2792−2796.
(47) Kaiser, T. E.; Wang, H.; Stepanenko, V.; Wurthner, F. Supramolecular Construction of Fluorescent J-Aggregates Based on Hydrogen-Bonded Perylene Dyes. *Angew. Chem., Int. Ed.* **2007**, *46*, 5541−5544.
(48) Perez, A.; Serrano, J. L.; Sierra, T.; Ballesteros, A.; Saa, D. D.; Barluenga, J. Control of Self-Assembly of a 3-Hexen-1,5-diyne Derivative: Toward Soft Materials with an Aggregation-Induced Enhancement in Emission. *J. Am. Chem. Soc.* **2011**, *133*, 8110−8113.
(49) Zujin, Z.; Lam, W. Y. J.; Tang, B. Z. Self-assembly of Organic Luminophores with Gelation-enhanced Emission Characteristics. *Soft Matter* **2013**, *9*, 4564−4579.
(50) Zhang, W.; Yuan, C.; Guo, J.; Qiu, L.; Yan, F. Supramolecular Ionic Liquid Gels for Quasi-Solid-State Dye-sensitized Solar Cells. *ACS Appl. Mater. Interfaces* **2014**, *6*, 8723−8728.
(51) Stupp, S. I.; LeBonheur, V.; Walker, K.; Li, L. S.; Huggins, K. E.; Keser, M.; Amstutz, A. Supramolecular Materials: Self-Organized Nanostructures. *Science* **1997**, *276*, 384−389.
(52) Bandela, A.; Chinta, J. P.; Hinge, V. K.; Dikundwar, A.; Guru Row, T. N.; Rao, C. P. Recognition of Polycyclic Aromatic Hydrocarbons and Their Derivatives by 1,3-Di-naphthalimide Cnjugate of Calix[4]arene: Emission, Absorption, Crystal Structures and Computational Studies. *J. Org. Chem.* **2011**, *76*, 1742−1750.
(53) Frisch, M. J.; Trucks, G. W.; Schlegel, H. B.; Scuseria, G. E.; Robb, M. A.; Cheeseman, J. R.; Montgomery, J. A., Jr., Vreven, T.; Kudin, K. N.; Burant, J. C.; Millam, J. M.; Iyengar, S. S.; Tomasi, J.; Barone, V.; Mennucci, B.; Cossi, M.; Scalmani, G.; Rega, N.; Petersson, G. A.; Nakatsuji, H.; Hada, M.; Ehara, M.; Toyota, K.; Fukuda, R.; Hasegawa, J.; Ishida, M.; Nakajima, T.; Honda, Y.; Kitao, O.; Nakai, H.; Klene, M.; Li, X.; Knox, J. E.; Hratchian, H. P.; Cross, J. B.; Adamo, C.; Jaramillo, J.; Gomperts, R.; Stratmann, R. E.; Yazyev, O.; Austin, A. J.; Cammi, R.; Pomelli, C.; Ochterski, J. W.; Ayala, P. Y.; Morokuma, K.; Voth, G. A.; Salvador, P.; Dannenberg, J. J.; Zakrzewski, V. G.; Dapprich, S.; Daniels, A. D.; Strain, M. C.; Farkas, O.; Malick, D. K.; Rabuck, A. D.; Raghavachari, K.; Foresman, J. B.; Ortiz, J. V.; Cui, Q.; Baboul, A. G.; Clifford, S.; Cioslowski, J.; Stefanov, B. B.; Liu, G.; Liashenko, A.; Piskorz, P.; Komaromi, I.; Martin, R. L.; Fox, D. J.; Keith, T.; Al-Laham, M. A.; Peng, C. Y.; Nanayakkara, A.; Challacombe, M.; Gill, P. M. W.; Johnson, B.; Chen, W.; Wong, M. W.; Gonzalez, C.; Pople, J. A. *Gaussian 03*, revision C.02; Gaussian, Inc.: Wallingford, CT, 2004.
(54) *Hyperchem 8.0.4*; Hypercube, Inc.: Gainesville, FL, 2007.

DOI: 10.1021/acsami.5b02506
ACS Appl. Mater. Interfaces 2015, 7, 11555−11566